PPARγ-K107 SUMOylation regulates insulin sensitivity but not adiposity in mice

Takeshi Katafuchi[a], William L. Holland[b,1], Rahul K. Kollipara[c], Ralf Kittler[a,c,d,e], David J. Mangelsdorf[a,f,2], and Steven A. Kliewer[a,g,2]

[a]Department of Pharmacology, UT Southwestern Medical Center, Dallas, TX 75390; [b]Touchstone Diabetes Center, Department of Internal Medicine, UT Southwestern Medical Center, Dallas, TX 75390; [c]Eugene McDermott Center for Human Growth and Development, UT Southwestern Medical Center, Dallas, TX 75390; [d]Simmons Comprehensive Cancer Center, UT Southwestern Medical Center, Dallas, TX 75390; [e]Green Center for Reproductive Biology, UT Southwestern Medical Center, Dallas, TX 75390; [f]Howard Hughes Medical Institute, UT Southwestern Medical Center, Dallas, TX 75390; and [g]Department of Molecular Biology, UT Southwestern Medical Center, Dallas, TX 75390

This contribution is part of the special series of Inaugural Articles by members of the National Academy of Sciences elected in 2015.

Contributed by Steven A. Kliewer, October 15, 2018 (sent for review August 23, 2018; reviewed by Bruce M. Spiegelman and Peter Tontonoz)

The nuclear receptor peroxisome proliferator-activated receptor γ (PPARγ) is a master regulator of adipocyte differentiation and is the target for the insulin-sensitizing thiazolidinedione (TZD) drugs used to treat type 2 diabetes. In cell-based in vitro studies, the transcriptional activity of PPARγ is inhibited by covalent attachment of small ubiquitin-related modifier (SUMOylation) at K107 in its N terminus. However, whether this posttranslational modification is relevant in vivo remains unclear. Here, using mice homozygous for a mutation (K107R) that prevents SUMOylation at this position, we demonstrate that PPARγ is SUMOylated at K107 in white adipose tissue. We further show that in the context of diet-induced obesity PPARγ-K107R–mutant mice have enhanced insulin sensitivity without the corresponding increase in adiposity that typically accompanies PPARγ activation by TZDs. Accordingly, the PPARγ-K107R mutation was weaker than TZD treatment in stimulating adipocyte differentiation in vitro. Moreover, we found that both the basal and TZD-dependent transcriptomes of inguinal and epididymal white adipose tissue depots were markedly altered in the K107R-mutant mice. We conclude that PPARγ SUMOylation at K107 is physiologically relevant and may serve as a pharmacologic target for uncoupling PPARγ's beneficial insulin-sensitizing effect from its adverse effect of weight gain.

PPARγ | SUMOylation | adipose tissue | insulin | rosiglitazone

Peroxisome proliferator-activated receptor γ (PPARγ) is a member of the nuclear receptor family of ligand-activated transcription factors that is activated by various fatty acids and their metabolites (1). Two forms of PPARγ, PPARγ1 and PPARγ2, which differ by a 30-aa N-terminal extension in PPARγ2, are derived from alternative promoter usage and mRNA splicing of the *PPARG* gene. While PPARγ1 is expressed at low levels in many tissues, PPARγ2 is enriched in adipocytes, where it serves as a master regulator of fat cell differentiation (1). In mature adipocytes, PPARγ2 regulates a program of genes involved in glucose and lipid homeostasis. Mutations in PPARγ cause lipodystrophy and severe insulin resistance in humans, and PPARγ is the molecular target for the thiazolidinedione (TZD) diabetes drugs, including rosiglitazone and pioglitazone (1, 2). Thus, PPARγ regulates systemic insulin sensitivity.

The transcriptional activity of PPARγ is regulated by a variety of posttranslational modifications including covalent attachment of small ubiquitin-related modifier (SUMO) to either K107 in the N terminus or K395 in the ligand-binding domain (numbering according to PPARγ2 sequence) (3). PPARγ SUMOylation at K107 strongly represses PPARγ transcriptional activity in vitro even though only a small percentage of PPARγ protein is modified (4–6). The mechanism may involve either recruitment of corepressor proteins or dissociation of coactivator proteins. Ligand-dependent PPARγ SUMOylation at K395 occurs in macrophages, where it is believed to target PPARγ to genes involved in inflammation to inhibit clearance of corepressor complexes, thereby maintaining the genes in a repressed state (7).

The metabolic regulatory hormone FGF21 is induced by TZDs and fasting/refeeding in white adipocytes, where it stimulates glucose uptake and insulin sensitivity (8, 9). We previously reported a positive regulatory loop wherein FGF21 activates PPARγ in isolated adipocytes by inhibiting its SUMOylation at K107 (10). However, whether K107 SUMOylation regulates PPARγ transcriptional activity in vivo remains unclear. In this report we evaluate the physiologic consequences of mutating K107 to prevent PPARγ SUMOylation at this residue in mice.

Results

K107R Mice Have Increased Insulin Sensitivity. Mice with a lysine-to-arginine substitution at codon 107 of PPARγ were generated by homologous recombination. Mice heterozygous and homozygous for the K107R mutation were born at the expected Mendelian

Significance

Covalent attachment of small ubiquitin-related modifier (SUMOylation) is a posttranslational modification that regulates the activity of many transcription factors. The nuclear receptor peroxisome proliferator-activated receptor gamma (PPARγ) is a master regulator of adipogenesis and the target of the thiazolidinedione (TZD) diabetes drugs. Although the TZDs have potent insulin-sensitizing properties, their use is limited by adverse effects such as weight gain. Here we provide unequivocal evidence that PPARγ is SUMOylated in mice at lysine-107 and that preventing this modification selectively enhances the insulin-sensitizing activity of PPARγ by regulating the expression of a discriminate network of genes in white adipose tissue. Our work suggests that inhibiting PPARγ SUMOylation may be a strategy for designing safer PPARγ drugs.

Author contributions: T.K., W.L.H., R.K., D.J.M., and S.A.K. designed research; T.K., W.L.H., and R.K.K. performed research; T.K., W.L.H., R.K.K., R.K., D.J.M., and S.A.K. analyzed data; T.K., R.K., D.J.M., and S.A.K. wrote the paper; and D.J.M. and S.A.K. supervised the project.

Reviewers: B.M.S., Harvard Medical School; and P.T., University of California, Los Angeles.

The authors declare no conflict of interest.

Data deposition: RNA-sequencing data have been deposited in the National Center for Biotechnology Information Gene Expression Omnibus databank (accession no. GSE120332).

See QnAs on page 12081.

[1]Present address: Department of Nutrition and Integrative Physiology, University of Utah College of Health, Salt Lake City, UT 84112.

[2]To whom correspondence may be addressed. Email: davo.mango@utsouthwestern.edu or steven.kliewer@utsouthwestern.edu.

This article contains supporting information online at www.pnas.org/lookup/suppl/doi:10.1073/pnas.1814522115/-/DCSupplemental.

Published online November 12, 2018.

ratio and appeared normal and healthy. Total PPARγ levels were unchanged in inguinal and epididymal white adipose tissue (iWAT and eWAT, respectively) and in interscapular brown adipose tissue (BAT) in heterozygous and homozygous K107R mice (Fig. 1*A*). However, SUMOylated PPARγ levels were reduced by half in iWAT and eWAT in heterozygous K107R mice and were virtually undetectable in homozygous K107R mice (Fig. 1*A*). We did not detect SUMOylated PPARγ in BAT (Fig. 1*A*). Phosphorylation at S112, which inhibits PPARγ transcriptional activity at least in part by enhancing K107 SUMOylation (11), was unaffected by the K107R mutation (Fig. 1*A*). These data demonstrate that PPARγ is SUMOylated in vivo and that there is little or no SUMOylation of PPARγ on residues other than K107 in adipose tissue.

Homozygous K107R mice (hereafter referred to as "K107R mice") fed a normal chow diet had body weights that were indistinguishable from WT littermates (Table 1). The K107R mice had a modest decrease in fasted plasma glucose concentrations but no changes in plasma insulin, triglyceride, nonesterified fatty acid (NEFA), cholesterol, adiponectin, or leptin levels (Table 1). When challenged with a high-fat diet, K107R mice gained slightly less weight than their WT littermates (Fig. 1*B* and Table 1) without accompanying changes in either adiposity or lean mass (Fig. 1*C*). This result was unexpected, given that PPARγ activation with TZDs causes weight gain due to increased adiposity and fluid retention (1, 2). After 19 wk on the high-fat diet, there were no differences between WT and K107R mice in plasma glucose, triglyceride, cholesterol, adiponectin, or leptin concentrations (Table 1), nor were there changes in iWAT or eWAT histology (Fig. 1*D*). Notably, however, the diet-induced obese (DIO) K107R mice had lower plasma insulin and NEFA levels than their WT littermates (Table 1).

To determine whether the K107R mutation affects insulin sensitivity, we performed hyperinsulinemic–euglycemic clamp

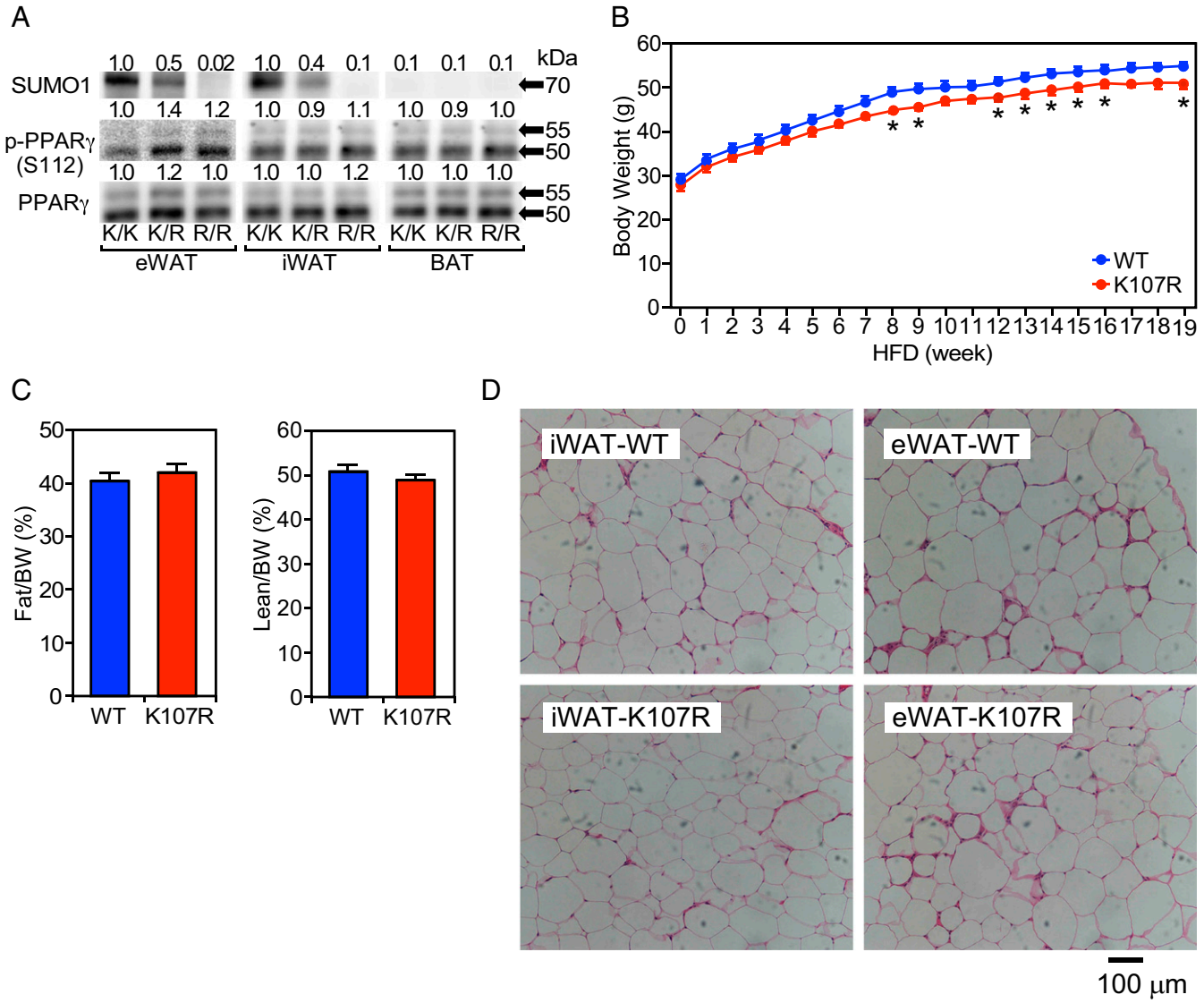

Fig. 1. PPARγ is SUMOylated at K107 in WAT. (*A*) Immunoblotting for SUMO1-conjugated PPARγ (SUMO1), S112-phosphorylated PPARγ (p-PPARγ), and total PPARγ following PPARγ immunoprecipitation from eWAT and iWAT and interscapular BAT from individual WT (K/K), K107R heterozygous (K/R), and homozygous (R/R) mutant mice. Band intensities were quantified by ImageJ and normalized to WT except for SUMO1-PPARγ levels in BAT, which were normalized to SUMO1 in WT iWAT. Molecular mass is indicated on the right. (*B*) Body weights of WT and homozygous K107R mice fed a high-fat diet (HFD) for the indicated times. (*C*) Fat and lean content of WT and homozygous K107R mice after 19 wk on a high-fat diet. Values were normalized to body weight. (*D*) H&E staining of iWAT and eWAT from WT and homozygous K107R mice after 19 wk on a high-fat diet. For *B* and *C*, $n = 6$ mice per group. $^*P < 0.05$.

Table 1. Metabolic parameters in PPARγ-K107R mice

Parameter	WT mice on chow diet	K107R mice on chow diet	*P* value	DIO WT mice	DIO K107R mice	*P* value
Body weight, g	30.3 ± 2.6	25.3 ± 1.1	0.12	55.3 ± 2.4	49.3 ± 1.0	0.030*
Glucose, mg/dL	135 ± 4.7	120 ± 4.1	0.032*	167 ± 7.6	175 ± 7.5	0.51
Insulin, ng/mL	1.00 ± 0.25	0.94 ± 0.13	0.84	2.09 ± 0.27	1.37 ± 0.15	0.036*
Cholesterol, mg/dL	150 ± 13.8	126 ± 13.4	0.25	202 ± 15.9	181 ± 22.0	0.44
Triglyceride, mg/mL	25.7 ± 2.0	29.7 ± 1.5	0.25	96.9 ± 22.5	77.9 ± 5.4	0.39
NEFA, mEq/mL	0.715 ± 0.046	0.562 ± 0.088	0.15	0.817 ± 0.055	0.624 ± 0.028	0.0069**
Adiponectin, mg/mL	10.6 ± 1.8	9.4 ± 1.3	0.33	11.9 ± 1.5	10.6 ± 0.60	0.40
Leptin, ng/mL	6.41 ± 2.57	2.57 ± 0.84	0.18	64.4 ± 6.3	60.2 ± 11.7	0.71

$n = 5$ to 8 mice per group.
*$P < 0.05$.
**$P < 0.01$.

experiments using weight-matched DIO WT (55.2 ± 1.9 g) and K107R (53.8 ± 2.5 g) mice. K107R mice had a doubling in both the glucose infusion rate and whole-body glucose uptake rate (Fig. 2*A*). There were significant increases in glucose uptake into gastrocnemius and diaphragm muscle and iWAT and similar trends in soleus muscle and eWAT, iWAT, and BAT (Fig. 2*B*). There was no difference between WT and K107R mice in basal glucose production (Fig. 2*A*). Thus, preventing PPARγ SUMOylation increases whole-body insulin sensitivity by stimulating glucose disposal principally in muscle.

Comparison of K107R and Rosiglitazone Effects in Vivo. To examine the relationship between PPARγ regulation by SUMOylation and TZDs, DIO WT and K107R mice were administered rosiglitazone or vehicle for 1 wk by oral gavage, and plasma insulin, glucose, triglycerides, NEFAs, and adiponectin concentrations

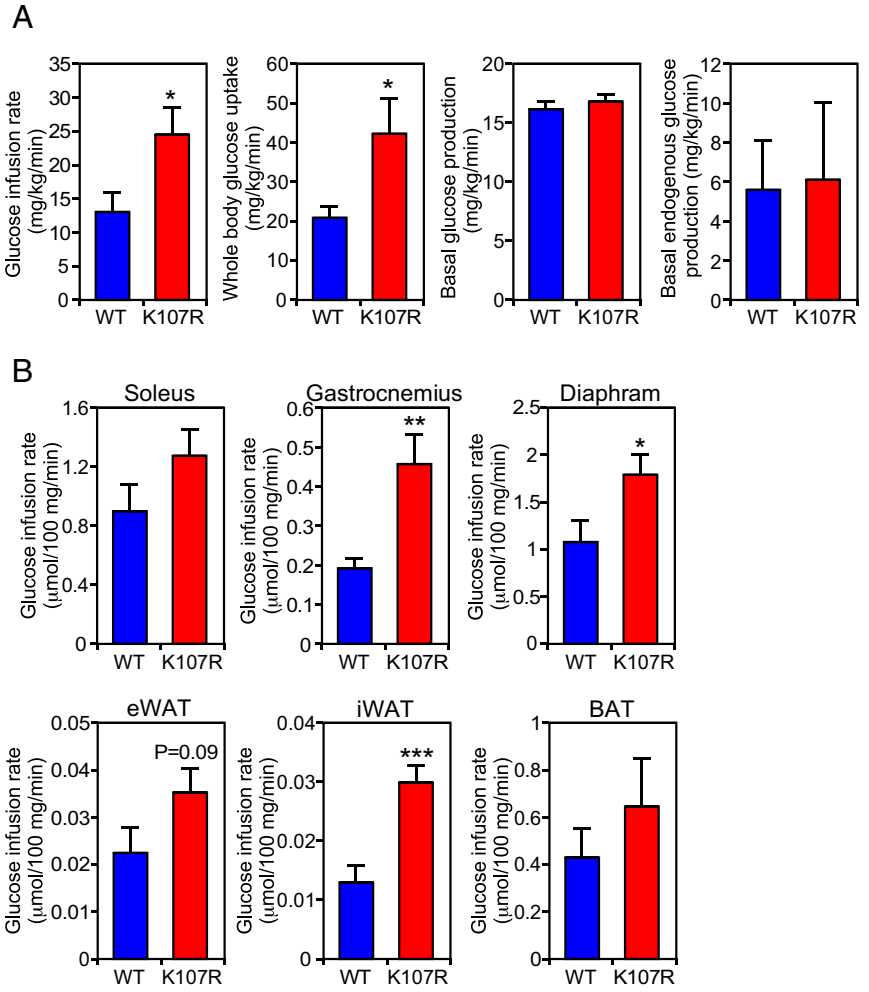

Fig. 2. K107R mice have increased insulin sensitivity. (*A*) Glucose infusion rate, whole-body glucose uptake, basal glucose production, and basal endogenous glucose production were measured under hyperinsulinemic–euglycemic clamp conditions in DIO WT and K107R mice. (*B*) Glucose uptake under clamp conditions into muscle depots (*Upper Row*) and in eWAT, iWAT, and BAT (*Lower Row*). $n = 8$ or 9 mice per group. *$P < 0.05$; **$P < 0.01$; ***$P < 0.001$.

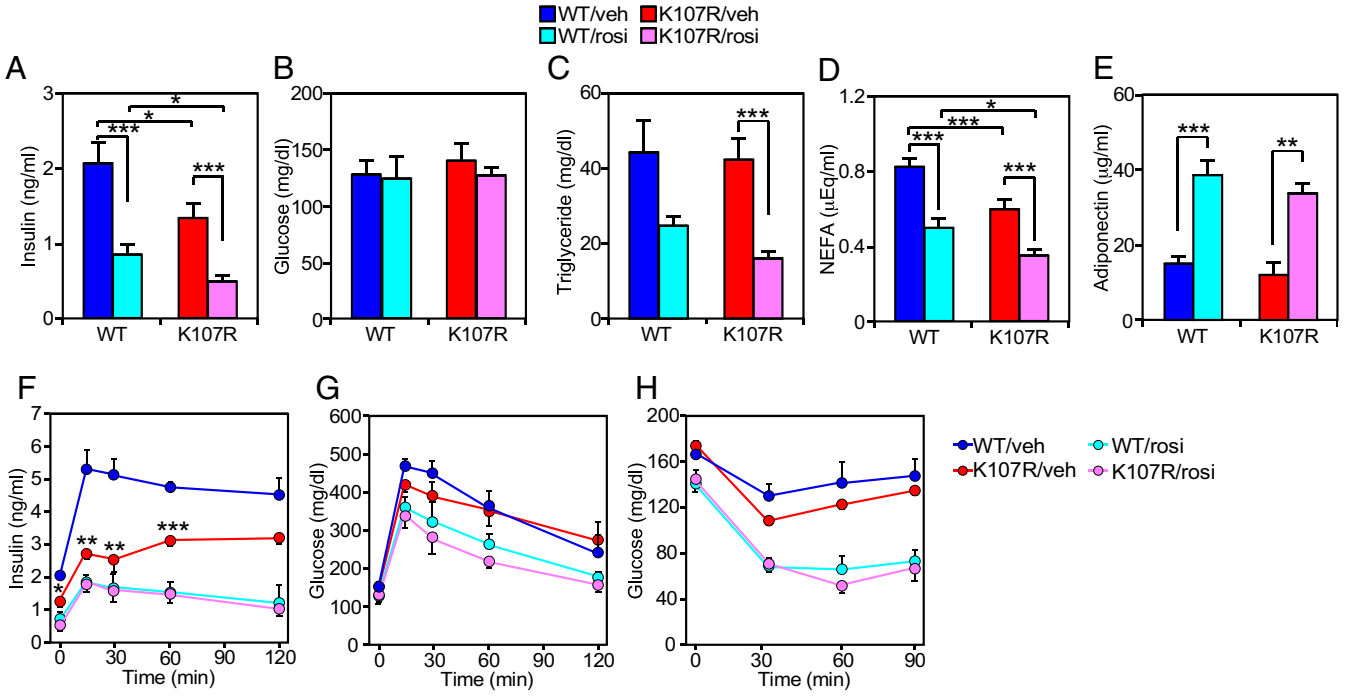

Fig. 3. Metabolic effects of K107R and rosiglitazone treatment. (*A–E*) Metabolic parameters were measured in plasma from DIO WT and K107R mice treated with vehicle (veh) or rosiglitazone (rosi) for 7 d by oral gavage. Blood was collected from the tail veins of 4-h–fasted mice to measure insulin and glucose or from the cardiac ventricle to measure other parameters. $n = 6$ mice per group. *$P < 0.05$; **$P < 0.01$; ***$P < 0.001$. (*F* and *G*) Plasma insulin (*F*) and glucose (*G*) concentrations during an i.p. glucose tolerance test in DIO WT and K107R mice treated with vehicle or rosiglitazone for 7 d by oral gavage. $n = 6$ mice per group. *$P < 0.05$; **$P < 0.01$; ***$P < 0.001$ compared with WT/veh mice. (*H*) Plasma glucose concentrations during an i.p. insulin tolerance test in DIO WT and K107R mice treated with vehicle or rosiglitazone for 7 d by oral gavage. $n = 6$ mice per group.

were measured (Fig. 3 *A–E*). As expected, K107R mice had lower plasma insulin and NEFA levels, which were further reduced by rosiglitazone treatment (Fig. 3 *A* and *D*). The K107R mice had no changes in plasma glucose, triglycerides, or adiponectin (Fig. 3 *B*, *C*, and *E*). Rosiglitazone treatment lowered plasma triglyceride levels and increased adiponectin levels to a comparable degree in both WT and K107R mice (Fig. 3 *C* and *E*). Thus, blocking SUMOylation and administering rosiglitazone have additive effects on a subset of PPARγ-regulated metabolic parameters, including plasma insulin and NEFA levels. Rosiglitazone has additional effects on plasma triglyceride and adiponectin concentrations that were not seen in K107R mice.

In an i.p. glucose tolerance test, K107R mice had decreased plasma insulin concentrations compared with WT mice (Fig. 3*F*). While plasma insulin concentrations decreased further in K107R mice treated with rosiglitazone, they were the same as those in WT mice administered rosiglitazone (Fig. 3*F*). Plasma glucose concentrations were also decreased to a similar extent in WT and K107R mice administered rosiglitazone (Fig. 3*G*). In an insulin tolerance test, plasma glucose concentrations trended lower in K107R mice than in WT mice (Fig. 3*H*), consistent with the increased insulin sensitivity observed in the hyperinsulinemic–euglycemic clamp studies. Rosiglitazone treatment decreased plasma glucose levels even further in both WT and K107R mice (Fig. 3*H*). We conclude that while K107R improves insulin sensitivity and glucose tolerance, it is less efficacious than rosiglitazone treatment.

To further compare PPARγ regulation by SUMOylation and TZDs, we performed comprehensive whole-transcriptome RNA sequencing (RNA-seq) analysis with RNA prepared from iWAT and eWAT of DIO WT and K107R mice administered either rosiglitazone or vehicle for 1 wk. Using stringent criteria [≥ twofold or greater change in expression, false-discovery rate (FDR) ≤0.05], we identified genes whose expression was either increased or decreased by K107R (compared with WT/vehicle), rosiglitazone (compared with WT/vehicle), or K107R + rosiglitazone (compared with K107R/vehicle) (Datasets S1 and S2). In iWAT, 80, 108, and 233 genes were increased by K107R, rosiglitazone, and K107R + rosiglitazone, respectively (Fig. 4 *A* and *B*). While there was surprisingly little overlap in the genes induced by K107R or rosiglitazone alone, the two together induced an additional 153 genes (Fig. 4 *A* and *B*). In eWAT, many more genes were induced by K107R (406) than by rosiglitazone (67), with only 19 genes in common (Fig. 4 *C* and *D*). Combining K107R and rosiglitazone induced an additional 202 genes (Fig. 4 *C* and *D*). Among the genes induced by K107R alone in iWAT was *Fgf21* (Dataset S1), which likely contributes to K107R's insulin-sensitizing effect. Other metabolism-related genes induced by K107R alone in both iWAT and eWAT are elongation of very long-chain fatty acids-like 3 (*Elovl3*), HMG-CoA synthase 2 (*Hmgcs2*), perilipin 5, and serine palmitoyltransferase long-chain base subunit 3. Additional K107R-induced genes involved in carbohydrate and lipid metabolism are highlighted in Datasets S1 and S2.

In iWAT, the expression of 62, 105, and 375 genes was decreased by K107R, rosiglitazone, or K107R + rosiglitazone, respectively (Fig. 4 *A* and *B*). Combining K107R with rosiglitazone repressed an additional 288 genes not seen with either K107R or rosiglitazone alone. In eWAT, 174, 106, and 440 genes were repressed by K107R, rosiglitazone, or K107R + rosiglitazone, respectively; 439 genes were repressed only by the combination of K107R + rosiglitazone (Fig. 4 *C* and *D*). Thus, K107R and rosiglitazone act together to repress large numbers of genes.

As expected, gene set enrichment analysis (GSEA; FDR ≤0.05) showed that rosiglitazone induced genes involved in adipogenesis and lipid metabolism and repressed genes involved in inflammation and lymphocyte activation in both iWAT and eWAT (Fig. 4 *B* and *D* and Datasets S3 and S4). K107R enhanced rosiglitazone's

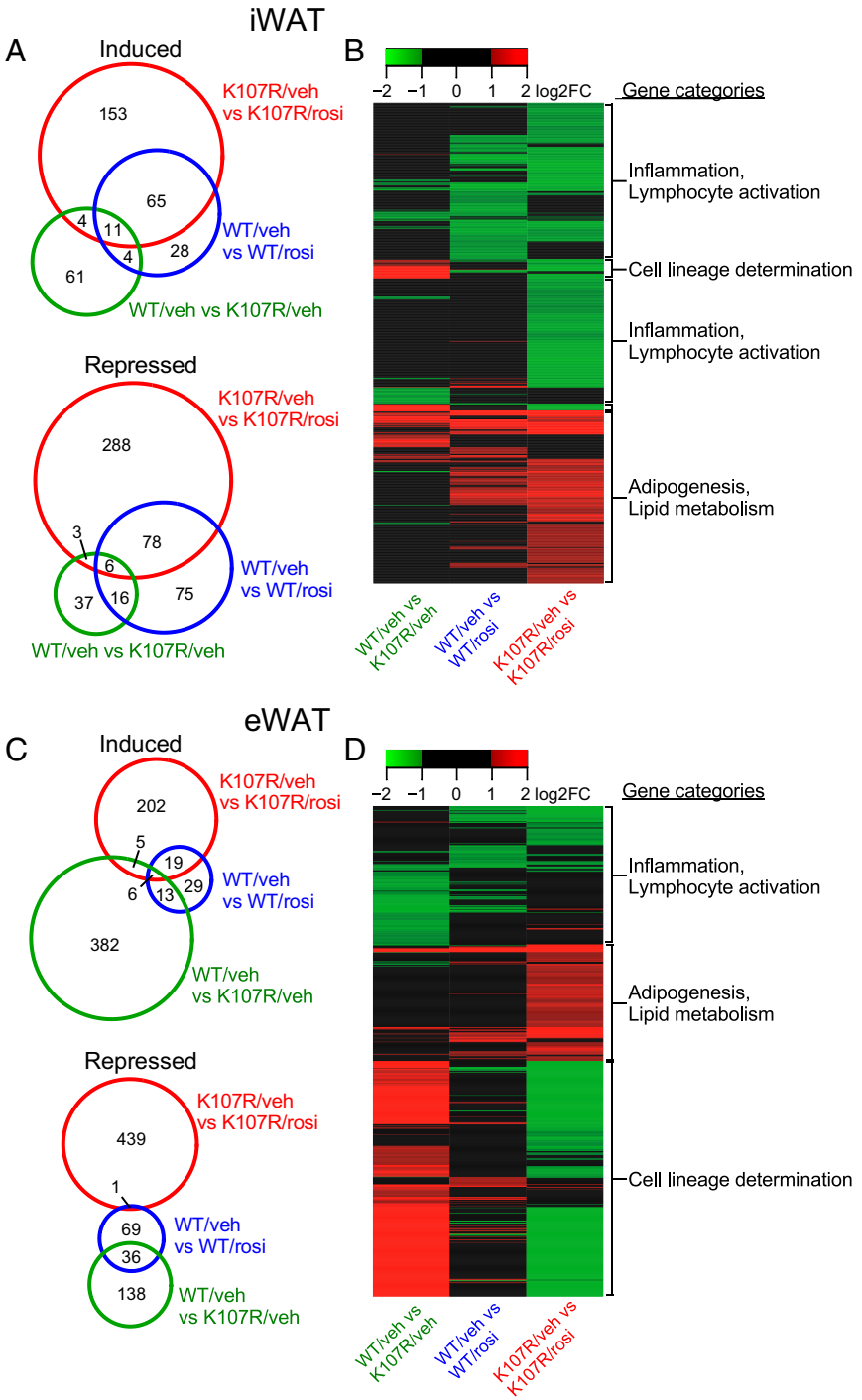

Fig. 4. RNA-seq analysis of iWAT and eWAT. RNA-seq analysis was performed using RNA prepared from iWAT or eWAT of WT and K107R mice treated with vehicle or rosiglitazone for 7 d by oral gavage. Criteria for gene selection were a twofold or greater change in expression and FDR ≤0.05. (*A* and *C*) Venn diagrams showing the number and overlap of genes whose expression was increased or decreased by K107R (relative to WT), rosiglitazone (relative to vehicle), or K107R + rosiglitazone (relative to K107R/vehicle). (*B* and *D*) Unsupervised hierarchical clustering analysis of the RNA-seq data summarized in *A* and *C*. Shown to the right of each panel are the major gene categories represented in the analysis as determined by GSEA (see Datasets S1 and S2 for a list of the differentially expressed genes in the K107R, rosiglitazone, and K107R + rosiglitazone comparisons in iWAT and eWAT, respectively, and Datasets S3 and S4 for a list of the names and statistics for the GSEA gene sets with the most positive or most negative enrichment scores for iWAT and eWAT, respectively).

inductive effects in both WAT depots (Fig. 4 *B* and *D*), consistent with its serving as a TZD sensitizer. The effects of K107R and rosiglitazone on inflammation genes were more complicated. In iWAT, the combination of K107R and rosiglitazone repressed many more inflammation-related genes than either did alone (Fig. 4*B*). However, this profile was not observed in eWAT (Fig. 4*D*), suggesting that K107R and rosiglitazone have depot-specific effects on inflammation.

Interestingly, K107R induced genes involved in cell lineage determination, including those related to muscle and kidney, in eWAT and to a lesser extent in iWAT (Fig. 4 *B* and *D* and Datasets S3 and S4). In contrast, these gene sets were unaffected

by rosiglitazone alone and were repressed by the combination of rosiglitazone and K107R (Fig. 4 *B* and *D*). These data reveal an unexpected combinatorial relationship between PPARγ SUMOylation and TZD binding in preventing the ectopic expression of transcripts normally present in other mesenchymal tissues. The biological significance of these intriguing findings remains to be determined.

Inductive Effects of K107R Are Adipocyte Autonomous. We examined the effect of K107R on adipocyte differentiation using stromal vascular cells derived from WT and K107R iWAT. Cells were differentiated using insulin, dexamethasone, and 3-isobutyl-1-methylxanthine (IBMX) in the absence or presence of rosiglitazone. In time-course studies, K107R had no significant effect on *Cepba*, *Cebpb*, and *Pparg* mRNA expression during the differentiation process (Fig. 5*A*). In contrast, rosiglitazone increased *Cepba* expression in WT cells on day 2 and *Cebpb* expression in both WT and K107R cells on days 6 and 8 (Fig. 5*A*). Accordingly, rosiglitazone accelerated neutral lipid accumulation compared with K107R, which had a more modest effect on its own (Fig. 5*B*). As expected, PPARγ was not SUMOylated in K107R adipocytes (Fig. 5*C*). Interestingly, PPARγ SUMOylation increased in response to rosiglitazone in WT adipocytes (Fig. 5*C*), supporting the existence of a feedback regulatory loop. We conclude that the K107R mutation has little effect on adipocyte differentiation in vitro.

We next sought to determine whether genes that are regulated by K107R in WAT in vivo are similarly regulated in isolated adipocytes in vitro. In an effort to recapitulate our in vivo conditions, stromal vascular cells were differentiated for 8 d using the insulin/dexamethasone/IBMX mixture and subsequently were incubated for 48 h in medium containing either vehicle or rosiglitazone. Based on our RNA-seq analysis, we selected genes from various groups shown in Fig. 4*A* that were induced by K107R and/or rosiglitazone in iWAT and compared their regulation in vivo and in vitro by qPCR. These genes included *Hmgcs2* (induced by K107R), integrin subunit alpha D (*Itgad*; induced by K107R), oxidized low-density lipoprotein receptor 1 (*Olr1*; induced by K107R + rosiglitazone), *Fgf21* (induced by K107R, K107R + rosiglitazone), enoyl-CoA hydratase and 3-hydroxyacyl CoA dehydrogenase (*Ehhadh*; induced by rosiglitazone, rosiglitazone + K107R), *Elovl3* (induced by K107R, rosiglitazone, K107R + rosiglitazone), and pyruvate dehydrogenase kinase 4 (*Pdk4*; induced by K107R, rosiglitazone, and K107R + rosiglitazone). Similar induction profiles in response to K107R and/or rosiglitazone were seen in iWAT, eWAT, and isolated iWAT adipocytes (Fig. 6*A*). Thus, K107R regulates the expression of these genes in an adipocyte-autonomous manner. Consistent with these findings, knockdown of the E2 ubiquitin conjugating enzyme, UBC9, which is required for PPARγ-K107 SUMOylation (4, 11), increased the expression of *Fgf21* and *Elovl3* in WT adipocytes but did not further increase the already elevated expression of these PPARγ target genes in K107R adipocytes (Fig. 6 *B* and *C*).

We performed a similar qPCR analysis on genes repressed by K107R and/or rosiglitazone in iWAT. These genes included GST alpha 3 (*Gsta3*; repressed by K107R), WNT1 inducible signaling pathway protein 2 (*Wisp2*; repressed by rosiglitazone), nerve growth factor (*Ngf*; repressed by K107R and rosiglitazone), BPI fold-containing family B member 6 (*Bpifb6*; repressed by K107R, rosiglitazone, and K107R + rosiglitazone), and nitric oxide synthase 2 (*Nos2*; repressed by K107R, rosiglitazone, and K107R + rosiglitazone). These genes showed the expected decrease in expression in response to K107R and/or rosiglitazone in iWAT and, with the exception of *Gsta3*, in eWAT (Fig. 7). The repression profile for *Gsta3* was reproduced in isolated adipocytes, while *Wisp2* showed a similar pattern of regulation in vitro and in vivo. However, the repression of *Ngf* and *Nos2* was not

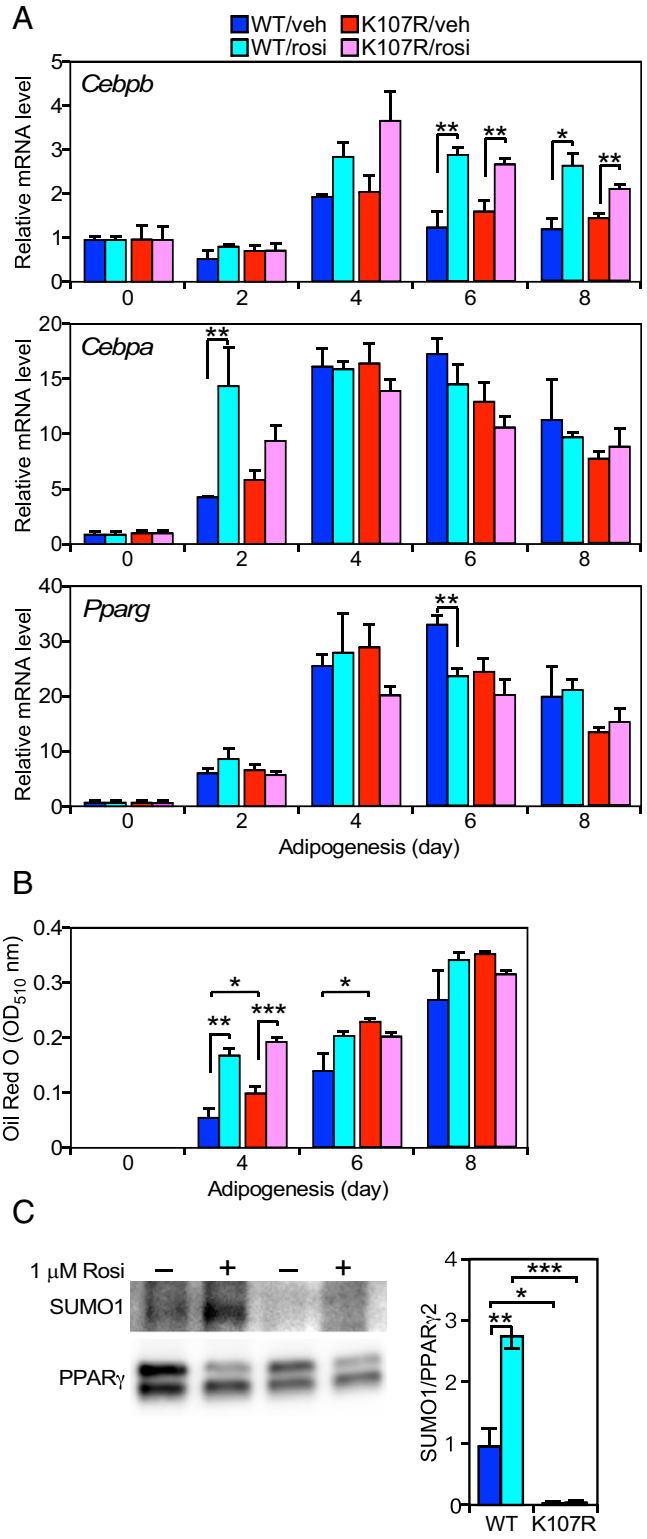

Fig. 5. In vitro analysis of K107R white adipocytes. (*A*) WT and K107R stromal vascular cells were differentiated using insulin, dexamethasone, and IBMX in the presence of rosiglitazone or vehicle. RNA was prepared at the indicated times, and *Cebpb*, *Cebpa*, and *Pparg* expression was measured by qPCR. (*B*) Neutral lipid accumulation was measured by Oil Red O staining at the indicated times. (*C*, *Left*) Immunoblotting for SUMO1-conjugated PPARγ (SUMO1) and total PPARγ following PPARγ immunoprecipitation. (*Right*) Quantification of SUMO1-conjugated PPARγ normalized to PPARγ2. $*P < 0.05$; $**P < 0.01$; $***P < 0.001$.

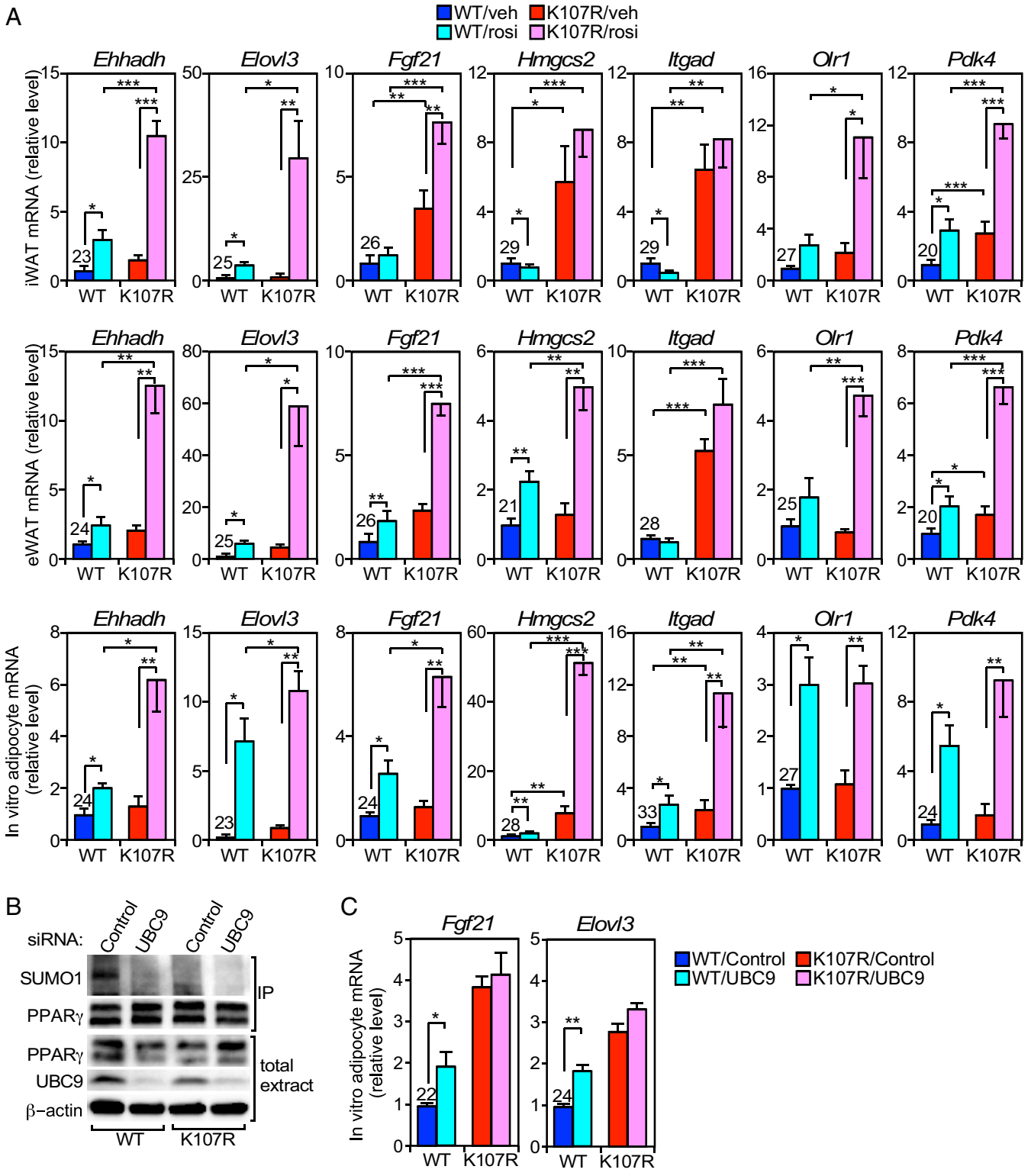

Fig. 6. K107R induces gene expression in an adipocyte-autonomous manner. (*A*) Comparison of gene regulation by K107R and rosiglitazone in vivo and in vitro. For the in vivo analysis, RNA was prepared from iWAT and eWAT from WT and K107R mice administered rosiglitazone or vehicle by oral gavage for 7 d. For the in vitro analysis, RNA was prepared from WT and K107R stromal vascular cells derived from iWAT and differentiated for 8 d using the insulin/dexamethasone/IBMX mixture and subsequently incubated for 48 h with either rosiglitazone or vehicle. Gene expression was measured by qPCR. Cycle threshold (Ct) values are shown for WT/vehicle conditions. (*B*) Immunoblotting for SUMO1-conjugated PPARγ (SUMO1) and total PPARγ following PPARγ immunoprecipitation (IP) (*Top Two Rows*) and total PPARγ, UBC9, and β-actin in total cell extract (*Bottom Three Rows*) from WT and K107R adipocytes treated with a control or UBC9 siRNA. (*C*) Quantification of *Fgf21* and *Elovl3* gene expression by qPCR using RNA prepared from WT and K107R adipocytes exposed to either the UBC9 or control siRNA. Ct values are shown for WT/control siRNA conditions. For *B* and *C*, WT and K107R stromal vascular cells were treated with control or UBC9 siRNA for 2 d in growth medium. The cells were subsequently incubated for 2 d in differentiation medium containing insulin, dexamethasone, IBMX, and rosiglitazone, followed by 2 d in medium containing only insulin and rosiglitazone. $*P < 0.05$; $**P < 0.01$; $***P < 0.001$.

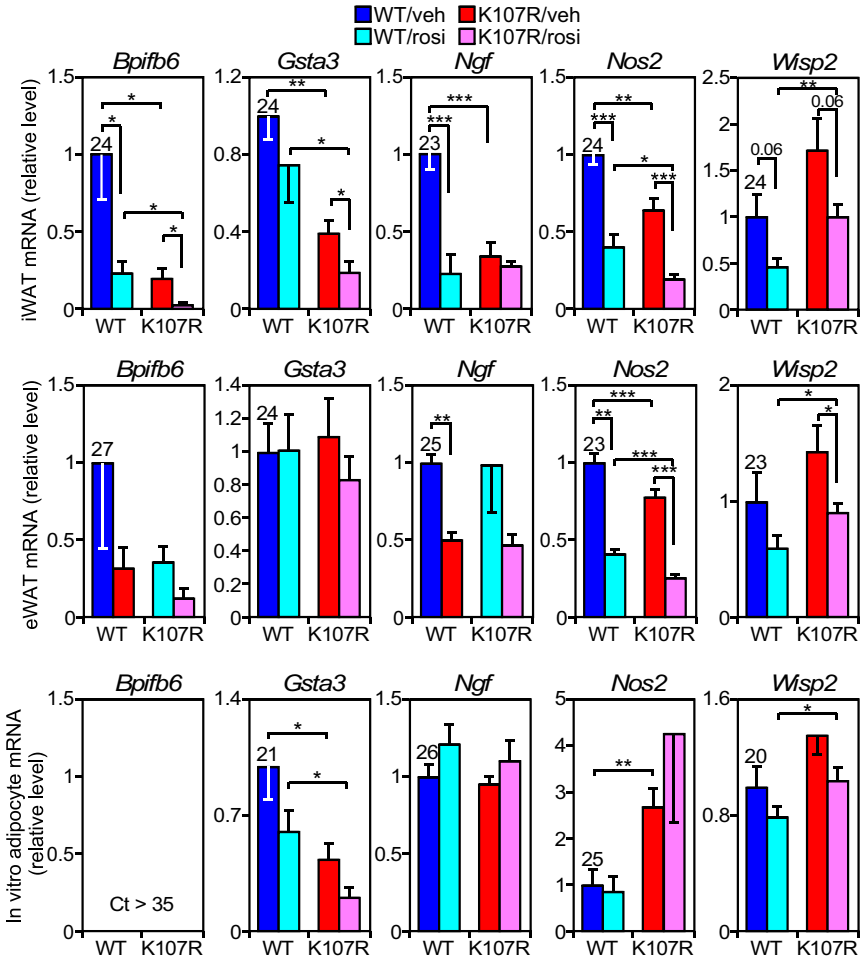

Fig. 7. Repression of gene expression by K107R and rosiglitazone is not consistently recapitulated in vitro. Comparison of gene regulation by K107R and rosiglitazone in vitro and in vivo, with the same samples as in Fig. 6*A*. Gene expression was measured by qPCR. Ct values are shown for WT/vehicle conditions. $*P < 0.05$; $**P < 0.01$; $***P < 0.001$.

recapitulated in vitro, and *Bpifb6* mRNA was below the limits of detection in isolated adipocytes (Fig. 7). We conclude that K107R and rosiglitazone can repress gene expression through either adipocyte-autonomous or adipocyte-nonautonomous mechanisms of action, depending on the gene.

Discussion

K107 SUMOylation markedly inhibits PPARγ transcriptional activity in vitro (4–6). However, whether PPARγ K107 SUMOylation is relevant in vivo has remained unclear: While we previously showed that FGF21 inhibits PPARγ SUMOylation in murine WAT (10), another group failed to detect SUMOylated PPARγ under similar conditions (12). Here, using homozygous K107R mice, we demonstrate unequivocally that PPARγ is SUMOylated in WAT and that this posttranslational modification has significant physiologic consequences. Among the genes induced by K107R in WAT was *Fgf21*. Thus, the FGF21–PPARγ pathway is a self-reinforcing regulatory loop.

K107R recapitulates a subset of rosiglitazone's and FGF21's metabolic actions in DIO mice. These include reducing plasma NEFA concentrations and increasing insulin sensitivity. However, unlike rosiglitazone and FGF21, K107R did not induce circulating adiponectin concentrations, nor did it decrease plasma triglyceride levels. In glucose tolerance and insulin tolerance assays, K107R was less efficacious than rosiglitazone. Interestingly, unlike TZDs, which cause weight gain by increasing adiposity and fluid retention (1, 2), K107R modestly decreased body weight in mice fed a high-fat diet. We did not observe changes in histology or *Ucp1* mRNA levels in WAT from K107R mice, suggesting that browning of WAT is unlikely to be the mechanism. These findings suggest that it may be possible to pharmacologically uncouple PPARγ's insulin-sensitizing actions from weight gain by targeting PPARγ SUMOylation status.

RNA-seq studies with WAT revealed two interesting effects of blocking K107 SUMOylation. First, the K107R mutation sensitized WAT to rosiglitazone's induction of metabolism-related genes. Since FGF21 inhibits PPARγ SUMOylation, these data are consistent with previous studies showing that FGF21-KO mice are refractory to the insulin-sensitizing actions of TZDs (10) and that FGF21 and TZDs cooperate in inducing glucose uptake into adipocytes in vitro (13). Second, K107R caused ectopic expression of genes involved in the differentiation and function of other cell lineages (e.g., muscle and kidney). These findings suggest an unexpected role for PPARγ SUMOylation in repressing genes normally expressed in other tissues.

In addition to SUMOylation, PPARγ's transcriptional activity is also regulated by other posttranslational modifications, including phosphorylation. Like SUMOylation at K107, PPARγ phosphorylation at the nearby residue, S112, inhibits its transcriptional activity (1–3). In cell-based experiments, mutating S112 to prevent phosphorylation causes a corresponding decrease in PPARγ SUMOylation, indicating that PPARγ is regulated by a

coordinate phosphorylation–SUMOylation switch (11). Accordingly, there are strong similarities between K107R- and S112A-mutant mice (14). When challenged with a high-fat diet, both have reduced plasma NEFA levels and are refractory to diet-induced insulin resistance without weight gain. However, S112A mice also had increased plasma adiponectin concentrations and decreased plasma triglyceride concentrations (14), which we did not observe in K107R mice. In addition, we found no differences in S112 phosphorylation in K107R mice, indicating that SUMOylation does not regulate phosphorylation at this site. Thus, while PPARγ may be regulated similarly by phosphorylation and SUMOylation, S112 phosphorylation and K107 SUMOylation are also likely to have distinct physiologic effects.

PPARγ is also phosphorylated at S273 and acetylated at K268 and K293 in its ligand-binding domain (15, 16). These post-translational modifications are inhibited by the binding of rosiglitazone and other ligands. Interestingly, PPARγ modulator ligands that have little or no classic agonist activity but prevent S273 phosphorylation improve insulin sensitivity in obese mice without causing weight gain (17). Similarly, double K268R/K293R acetylation-mutant mice have increased energy expenditure and are protected against high-fat-diet–induced obesity through a mechanism involving the browning of WAT (16, 18). Thus, blocking PPARγ SUMOylation, phosphorylation, and acetylation all provide a means for separating PPARγ's beneficial metabolic actions from its adverse adipogenic effect.

In closing, we show that PPARγ is SUMOylated at K107 in WAT and that this regulates PPARγ transcriptional activity. We further demonstrate that the K107R mutation recapitulates the insulin-sensitizing actions of rosiglitazone, albeit with reduced efficacy, and that it enhances the effect of rosiglitazone on genes involved in metabolism. Importantly, K107R improves insulin sensitivity without increasing body weight or adiposity. Thus, inhibiting PPARγ K107 SUMOylation may provide a mechanism for generating novel PPARγ-targeted insulin-sensitizing drugs with fewer side effects.

Materials and Methods

Generation of PPARγ-K107R Mice. The PPARγ-K107R targeting vector was constructed using a recombineering-based method (19). A 10,268-bp genomic DNA fragment containing exons 2 and 3 of the *PPARγ2* gene was transferred from BAC clone RP23-207O20 to a vector containing the diphtheria toxin negative-selection gene. The point mutation corresponding to K107R was synthesized and cloned into the 5′ end of an frt-Neo-frt cassette. The lengths of the 5′ and 3′ homologous arms were 5,473 bp and 4,434 bp, respectively. The neo cassette was inserted in intron 3, 192 bp downstream of exon 3. The targeting vector was electroporated into F1 129S6 × C57BL/6J hybrid ES cells derived by the Janelia Transgenic Facility. The G418-resistant ES clones were screened by nested PCR using primers outside the construct paired with primers inside the inserted cassette. The primer sequences were 5′ arm forward primers, PPARγ2 Scr F1: GACACTGACTTACTCCTGAG and PPARγ2 Scr F2: TGACTTACAGCTTGGCAGCA. Reverse primers were PGK R1: TGGATGTGGAATGTGTGCGA and PGK R2 TAAAGCGCATGCTCCAGACT. The 3′ arm forward primers were Neo F3: CTTCCTCGTGCTTTACGGTA and Neo F4: ACGAGTTCTTCTGAGGGGAT. Reverse primers were PPARγ2 Scr R3: CTTGTTCTGGAAGTCCAGAC and PPARγ2: Scr R4 AATCCTGGCTCCATGTGGAA. The PCR^+ ES cells were aggregated with eight-cell CD-1 strain embryos. The neo cassette was removed by breeding germline chimeras with ROSA26FLP1 homozygous females (Jackson Laboratories stock no. 003946). Correct targeting was confirmed by via chimera × F1 heterozygous female matings. Mice were maintained on a rodent chow (TD.2916; Harlan Teklad) and were fed a high-fat diet (D12492i; Research Diets) to induce obesity. All animal experiments were approved by the Institutional Animal Research Advisory Committee of the UT Southwestern Medical Center at Dallas.

Plasma Measurements. WT and K107R mice fed the high-fat diet for 19 wk were fasted for 4 h, and blood was collected from the tail vein for measuring glucose and insulin or from the cardiac ventricle for measuring other parameters. Kits were used to measure plasma triglyceride (Infinity Triglyceride Kit; Thermo Fisher Scientific), NEFA (NEFA-HR Kit; Wako), cholesterol (Cholesterol-E Kit; Wako), and glucose (Autokit Glucose; Wako) concentrations. ELISA kits were used to measure insulin (Crystal Chem, Inc.) and adiponectin and leptin (Millipore).

Glucose Tolerance and Insulin Tolerance Tests. Glucose tolerance tests were performed on mice that were fasted for 16 h and i.p. injected with 2 g/kg glucose. Insulin tolerance tests were performed in mice that were fasted for 4 h and i.p. injected with 0.75 U/kg insulin (Sigma).

Hyperinsulinemic–Euglycemic Clamp Studies. Studies were performed as described (20) using WT and K107R mice fed the high-fat diet for 19 wk. Briefly, mice were fasted for 4 h before the experiments. At $t = -90$ min, continuous infusion of [^{3}H] 2-deoxyglucose (0.05 μCi/min) was started to measure glucose turnover, and basal blood samples were collected from the tail vein at $t = -15$ and $t = -5$ min. Continuous infusion of insulin (4 $mU \cdot kg^{-1} \cdot min^{-1}$) was started at $t = 0$ with the tracer infusion increased to 0.1 μCi/min. Blood glucose levels were monitored every 10 min, and the blood glucose concentration was maintained at ∼150 mg/dL by infusion of 50% dextrose. At steady state, between 80 and 120 min, tail vein blood was collected every 20 min to determine glucose turnover.

In Vitro Adipocyte Differentiation. Preadipocytes were derived from the stromal vascular fraction of neonate inguinal adipose tissue as described (10). Briefly, the isolated fat pads were digested with 0.2% collagenase II (Worthington) in HBSS containing 2% BSA at 37 °C for 1 h. The tissue was suspended by pipetting and centrifuged at 300 × *g* for 2 min to isolate preadipocytes at the bottom. The cells were rinsed once with DMEM growth medium containing 10% heat-inactivated FBS, 20 mM Hepes (pH 7.3), 1× nonessential amino acids (Thermo Fisher Scientific), 2 mM GlutaMAX (Thermo Fisher Scientific), and 0.1 mM 2-mercaptoethanol and were cultured on 35-mm dishes in growth medium for 5 d until the cells reached confluence. The cells were then transferred to 10-cm dishes or multiwell dishes and were cultured with the growth medium for another 5 d. Adipogenesis was induced by culturing cells for 2 d in DMEM containing 10% non–heat-inactivated FBS supplemented with 5 μg/mL bovine insulin (Sigma), 1 μM dexamethasone, and 0.5 mM IBMX followed by 6 d in DMEM + 10% FBS supplemented with insulin only with medium changes every other day. The culture medium was then switched to DMEM + 10% FBS supplemented with insulin containing 1 μM rosiglitazone or vehicle for 48 h. Differentiated adipocytes were used for RNA purification or protein extraction. For the adipocyte differentiation time-course study, cells were differentiated for 2 d in DMEM + 10% FBS supplemented with insulin, dexamethasone, and IBMX containing 1 μM rosiglitazone or vehicle followed by 6 d in DMEM + 10% FBS supplemented with insulin containing 1 μM rosiglitazone or vehicle. The medium was changed every other day. For neutral lipid measurements, 0.5% Oil Red O (Fisher Biotec) dissolved in 2-propanol was mixed with water at a ratio of 3:2 and filtered. Cells were fixed with 10% formalin at room temperature for 15 min, washed with PBS and 60% 2-propanol, and then stained with the Oil Red O staining solution. Following incubation at 37 °C for 1 h, cells were rinsed with 60% 2-propanol and water. Oil Red O in lipid droplets was captured with 100% 2-propanol, and its concentration was measured by absorbance at 510 nm.

Immunoprecipitation and Western Blot Analysis. Adipose tissue or isolated adipocytes were homogenized with radioimmunoprecipitation assay (RIPA) buffer containing 50 mM Tris (pH 8), 150 mM NaCl, 1 mM EDTA, 1% IGEPAL CA-630 (Sigma), 0.5% deoxycholic acid, 0.1% SDS, protease inhibitors (Sigma), phosphatase inhibitors (Roche), and 20 mM *N*-ethyl maleimide (NEM) and were snap-frozen in liquid nitrogen. The homogenates were defrosted at 4 °C with mild agitation overnight and were centrifuged at 3,000 × *g* for 15 min at 4 °C. The supernatants were centrifuged again at 18,000 × *g* for 15 min at 4 °C, and the resulting supernatants were precleaned using protein A/G agarose. Following centrifugation at 1,000 × *g* for 1 min, the supernatants were mixed with PPARγ antibody (sc-7273; Santa Cruz), incubated overnight at 4 °C with mild agitation, mixed with Protein A/G agarose beads, and incubated with mild agitation for 2 h at 4 °C. Following centrifugation at 1,000 × *g* for 1 min, the beads were washed once with RIPA buffer, twice with buffer containing 50 mM Tris (pH 7.4), 250 mM NaCl, 100 mM LiCl, 0.1% Triton X-100, 20 mM NEM, and protease and phosphatase inhibitors, and twice with buffer containing 20 mM Hepes (pH 7.4), 10 mM $MgCl_2$, 2 mM EDTA, 0.1% Triton X-100, and protease inhibitors. The beads were suspended in SDS/PAGE sample buffer without 2-mercaptoethanol, heated at 95 °C for 5 min, and filtered using Spin-X centrifuge tube filters (Costar). The immunoprecipitated samples and total extracts were resolved by SDS/PAGE and blotted onto a nitrocellulose membrane, and the proteins of interest were detected by antibodies against PPARγ

(no. 2435; Cell Signaling), SUMO-1 (no. 4940; Cell Signaling), β-actin (A5316; Sigma), and UBC9 (no. 4918; Cell Signaling).

RNA-Seq. Groups of K107R and WT littermates fed the high-fat diet for 19 wk were administered either vehicle (1% methylcellulose) or rosiglitazone (10 mg·kg^{-1}·d^{-1}) by oral gavage for 1 wk (n = 6 mice per group). Total RNA from iWAT or eWAT from each group was prepared, pooled, and run on an Agilent TapeStation 4200 system to confirm quality (RNA integrity number >8). RNA-seq libraries were generated using DNase-treated total RNA (4 μg) and the TruSeq Stranded mRNA kit (Illumina). Poly-A RNA was purified and fragmented, and cDNA was synthesized. cDNA was A-tailed, and indexed adapters were ligated. After ligation, samples were PCR amplified and purified with Ampure XP beads (Beckman Coulter), and the quality was confirmed using the Agilent TapeStation 4200 system. Before normalization and pooling, samples were quantified by Qubit and then were run on the Illumina NextSeq 500 sequencer using V2 reagents. Raw data were then demultiplexed and converted to FASTQ files using Bcl2fastq (v2.17; Illumina). The FASTQ files were checked for quality using FastQC (v0.11.2) (21) and FASTQ Screen (v0.4.4) (22). FASTQ files were mapped to the mm10 assembly of the mouse genome using TopHat (23); fragments per kilobase per million mapped reads (FPKM) calculation and differential expression analysis were performed using Cufflinks (v 2.2.1) (24). RNA-seq data have been deposited in the National Center for Biotechnology Information Gene Expression Omnibus databank (accession no. GSE120332). We used the union set of differentially expressed genes with fold change ≥2 and adjusted P value ≤ 0.05 across the three different comparisons (WT/vehicle vs. K107R/vehicle, WT/vehicle vs. WT/rosiglitazone, and K107R/vehicle vs. K107R/rosiglitazone) in iWAT or eWAT for visualization. Heatmaps were generated using log2-transformed fold changes, and hierarchical clustering was performed using the Euclidean distance metric and the ward.D2 method using the heatmap.2 function available in the *gplots* R package. To analyze the enrichment of gene sets in rank-ordered gene lists obtained for the expression changes in the three different comparisons in iWAT or eWAT samples, we performed GSEA (25). We used the signal-to-noise ratio metric to rank the genes.

qPCR. RNA from adipose tissue or isolated adipocytes was purified using the RNeasy Lipid Tissue Mini Kit (Qiagen) or RNA Stat-60 (Amsbio), respectively. cDNA was synthesized from 2 μg total RNA using High-capacity cDNA Transcription Kits (Thermo Fisher Scientific) with random primers. qPCR was performed with the primer sets listed in *SI Appendix*, Table S1.

RNAi. The control SMARTpool of nontargeting siRNA (D-001810-10-05) and siRNA specific for the RNA encoding UBC9 (*Ube2i*) (D-040661-02-0005) pooled with sequences GGGAAGGAGGCUUGUUCAA, GGUCCGAGCACAAGCGAAG, CUACACAAUUUACUGCCAA, and AGAUCUAAGUCGCUCCGUA were purchased from Dharmacon. Preadipocytes isolated from WT and K107R neonatal mice were seeded onto 10-cm or 24-well dishes and were cultured for 3 d. The siRNAs were transfected using Lipofectamine RNAiMAX transfection reagent (Thermo Fisher Scientific) with OptiMEM according to the manufacturer's protocol, and the siRNA-transfected cells were further cultured another 2 d. Adipogenesis was induced by culturing those cells for 2 d with DMEM supplemented with 10% non–heat-inactivated FBS, 5 mg/mL insulin, 1 μM dexamethasone, 0.5 mM IBMX, and 1 μM rosiglitazone followed by culturing for 2 d with DMEM + 10% FBS supplemented with insulin and rosiglitazone only. Immunoprecipitation and detection of proteins of interest were performed as described above by using the cells on 10-cm dishes. The cells on 24-well dishes were used for isolation of RNA for qPCR.

ACKNOWLEDGMENTS. We thank Yuan Zhang for expert technical assistance. This work was supported by NIH Grants R01DK108833 and R01DK112826 (to W.L.H.) and R01DK067158 and P01AG051459 (to D.J.M. and S.A.K.), Robert A. Welch Foundation Grants I-1558 (to S.A.K.) and I-1275 (to D.J.M.), and the Howard Hughes Medical Institute (D.J.M.). R.K. is a John L. Roach Scholar in Biomedical Research and a Cancer Prevention Research Institute of Texas Scholar in Cancer Research.

1. Tontonoz P, Spiegelman BM (2008) Fat and beyond: The diverse biology of PPARgamma. *Annu Rev Biochem* 77:289–312.
2. Soccio RE, Chen ER, Lazar MA (2014) Thiazolidinediones and the promise of insulin sensitization in type 2 diabetes. *Cell Metab* 20:573–591.
3. Floyd ZE, Stephens JM (2012) Controlling a master switch of adipocyte development and insulin sensitivity: Covalent modifications of PPARγ. *Biochim Biophys Acta* 1822: 1090–1095.
4. Ohshima T, Koga H, Shimotohno K (2004) Transcriptional activity of peroxisome proliferator-activated receptor gamma is modulated by SUMO-1 modification. *J Biol Chem* 279:29551–29557.
5. Shimada T, et al. (2004) Targeted ablation of Fgf23 demonstrates an essential physiological role of FGF23 in phosphate and vitamin D metabolism. *J Clin Invest* 113: 561–568.
6. Floyd ZE, Stephens JM (2004) Control of peroxisome proliferator-activated receptor gamma2 stability and activity by SUMOylation. *Obes Res* 12:921–928.
7. Pascual G, et al. (2005) A SUMOylation-dependent pathway mediates transrepression of inflammatory response genes by PPAR-gamma. *Nature* 437:759–763.
8. Potthoff MJ, Kliewer SA, Mangelsdorf DJ (2012) Endocrine fibroblast growth factors 15/19 and 21: From feast to famine. *Genes Dev* 26:312–324.
9. BonDurant LD, Potthoff MJ (2018) Fibroblast growth factor 21: A versatile regulator of metabolic homeostasis. *Annu Rev Nutr* 38:173–196.
10. Dutchak PA, et al. (2012) Fibroblast growth factor-21 regulates PPARγ activity and the antidiabetic actions of thiazolidinediones. *Cell* 148:556–567.
11. Yamashita D, et al. (2004) The transactivating function of peroxisome proliferator-activated receptor gamma is negatively regulated by SUMO conjugation in the amino-terminal domain. *Genes Cells* 9:1017–1029.
12. Adams AC, et al. (2013) Fibroblast growth factor 21 is not required for the antidiabetic actions of the thiazoladinediones. *Mol Metab* 2:205–214.
13. Moyers JS, et al. (2007) Molecular determinants of FGF-21 activity-synergy and cross-talk with PPARgamma signaling. *J Cell Physiol* 210:1–6.
14. Rangwala SM, et al. (2003) Genetic modulation of PPARgamma phosphorylation regulates insulin sensitivity. *Dev Cell* 5:657–663.
15. Choi JH, et al. (2010) Anti-diabetic drugs inhibit obesity-linked phosphorylation of PPARgamma by Cdk5. *Nature* 466:451–456.
16. Qiang L, et al. (2012) Brown remodeling of white adipose tissue by SirT1-dependent deacetylation of Pparγ. *Cell* 150:620–632.
17. Choi JH, et al. (2011) Antidiabetic actions of a non-agonist PPARγ ligand blocking Cdk5-mediated phosphorylation. *Nature* 477:477–481.
18. Kraakman MJ, et al. (2018) PPARγ deacetylation dissociates thiazolidinedione's metabolic benefits from its adverse effects. *J Clin Invest* 128:2600–2612.
19. Liu P, Jenkins NA, Copeland NG (2003) A highly efficient recombineering-based method for generating conditional knockout mutations. *Genome Res* 13:476–484.
20. Lan T, et al. (2017) FGF19, FGF21, and an FGFR1/β-Klotho-activating antibody act on the nervous system to regulate body weight and glycemia. *Cell Metab* 26:709–718.e3.
21. Andrews S (2014) *FastQC: A Quality Control Tool for High Throughput Sequence Data*. Available at www.bioinformatics.babraham.ac.uk/projects/fastqc/. Accessed November 1, 2018.
22. Wingett S (2011) *FastQ Screen: A Quality Control Tool to Screen a Library of Sequences in FastQ Format Against a Set of Sequence Databases*. Available at https://www.bioinformatics.babraham.ac.uk/projects/fastq_screen/. Accessed November 1, 2018.
23. Kim D, et al. (2013) TopHat2: Accurate alignment of transcriptomes in the presence of insertions, deletions and gene fusions. *Genome Biol* 14:R36.
24. Trapnell C, et al. (2010) Transcript assembly and quantification by RNA-seq reveals unannotated transcripts and isoform switching during cell differentiation. *Nat Biotechnol* 28:511–515.
25. Subramanian A, et al. (2005) Gene set enrichment analysis: A knowledge-based approach for interpreting genome-wide expression profiles. *Proc Natl Acad Sci USA* 102: 15545–15550.